Coastal Structures 2019 - Nils Goseberg, Torsten Schlurmann (eds) - © 2019 Bundesanstalt für Wasserbau
ISBN 978-3-939230-64-9 (Online) - DOI: 10.18451/978-3-939230-64-9_059

Simulations of Storm-Induced Erosion on an Embayed Beach

Ying-Chi Chen[1], Ching-Piao Tsai[2] & Chun-Han Ko[3]
[1]*Ph. D. candidate, Department of Civil Engineering, National Chung Hsing University, Taiwan*
[2]*Professor, Department of Civil Engineering, National Chung Hsing University, Taiwan*
[3]*Post Doctor Researcher, Department of Civil Engineering, National Chung Hsing University, Taiwan*

Abstract: The simulations of storm-induced erosion on a beach is an important issue nowadays in consideration of climate change impact. The appraisal formula of storm-induced erosion for a plane beach without coastal structure under the action of cyclonic waves can be found in the previous literatures where often one-dimensional Sbeach model simulation were used. This study applies a two-dimensional XBeach model to simulate the coastal topography change under storm wave action and estimate the storm-induced erosion on an embayed beach in which nearshore current circulation exists. The simulations for the equilibrium shoreline behind the breakwaters resulting from headland effects were first performed under seasonal wave conditions, showing in a good agreement with the empirical parabolic formula. The short-term change of the beach topography under the storm waves by considering different return periods of typhoons and geometric arrangements of breakwaters were then simulated, from which the storm-induced erosion widths on an embayed beach were analyzed. The numerical results show that the beach erosion increases with the increasing of the storm return period, which implies that the larger storm beach buffer width for larger cyclonic waves is needed for the coastal protection. Moreover, as the distance of the gap decreases (Xi/Gb=0.5~1.5), the shoreline after the storm will setback obviously and the larger storm beach buffer width will be needed due to the fiercer current system mainly.

Keywords: Storm-induced Erosion, XBEACH, embayed beach, nearshore current, coastal topography change

1 Introduction

Sandy beach supplies not only the coastal recreation areas but also the needed protection against the violent storm. To protect the property, habitat, and infrastructure development in the coastal city, the coastal structures, such as hard structures, such as seawall or detached breakwaters, have been constructed in many countries around the world as shown in Fig. 1. The pocket beaches or embayed beaches can be found on sandy coast between natural headlands or harbor construction, which extends an existing breakwater further into the sea. This arrangement has the potential to create a curve beach in the shadow zone of the structure due to the strongly coupled with the steering of wave-driven current which causes the cellular circulation patterns. The embayed beach shorelines by the headland control tend to be relatively stable over the long timescales, typically evolving toward an equilibrium configuration (Yasso, 1965; Silvester and Hsu, 1997).

However, despite the embayed beaches shoreline in static equilibrium were formed by many coastal protection countermeasures applied, the impact of storms on the beaches can cause the shoreline retreated by dramatic erosion over a short-term period. Beach erosion in some countries became apparent during sporadic storm events, which impacted the stability of equilibrium beach configuration. For example, Hurricane Ivan attacked the northwestern Florida and Alabama coast on September 16, 2004. Wang et al. (2006) examined the beach erosion during storm impact, and about 75m of beach width was eroded by Hurricane Ivan between 14 and 24 September 2004, as shown in Fig. 2. Many coastal scientists have acknowledged the benefit of providing a wide, healthy sandy

beach which can reduce the storm wave energy and protect the in upland property and infrastructure in a coastal zone (Lin et al., 2011). The National Research Council in the United States has recommended local coastal setback for construction in a coastal hazard zone shown in Fig. 3, that the readily movable smaller structures and large structures should be located behind the 30-year projection line (E-30 line) and the 60-year projection line (E-60 line), respectively (Dean and Darlymple, 2002).

Consequently, the appraisal of erosion width by storms is one of the most important issues nowadays in coastal engineering in consideration of storm surge impact. The storm waves determine the destructive potential of a storm, while the range in water level also influences the erosion potential. The coastal disaster will happen due to the storm-induced erosion due to the lack of sufficient sandy beach width. Lee et al. (2011) evaluated the storm beach buffer width by considering the different storm return periods and design water levels based on the simulations by one-dimensional model. However, the storm-induced erosion was associated with the development of the wave-driven circulation patterns and embayment nearshore current (Loureiro et al., 2012; Daly et al., 2014). The one-dimensional model mentioned above is only oriented towards onshore and offshore current, which may be not suitable for the situation as longshore current and rip current strongly co-exists. Therefore, this study is aimed to apply a two-dimensional XBeach model (Kingsday release version) to simulate the coastal morphology change during storms and estimate the appropriate erosion width with the different geometric arrangements of the headland-breakwater system. Additionally, The study also calculates the wave characteristic and nearshore current which are the main forcing mechanisms to control the sediment transport. The numerical results can be for the adaptation strategies to the storm waves impact on an embayed beach in the future.

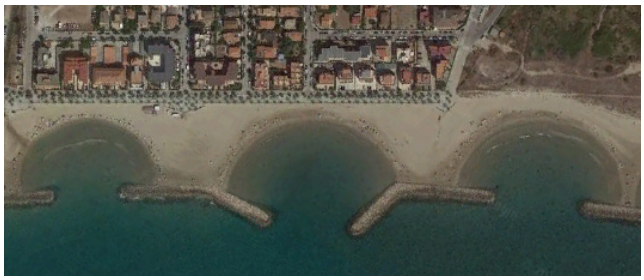

Fig. 1. Barcelona coast, Spain. (Photo by: Google earth)

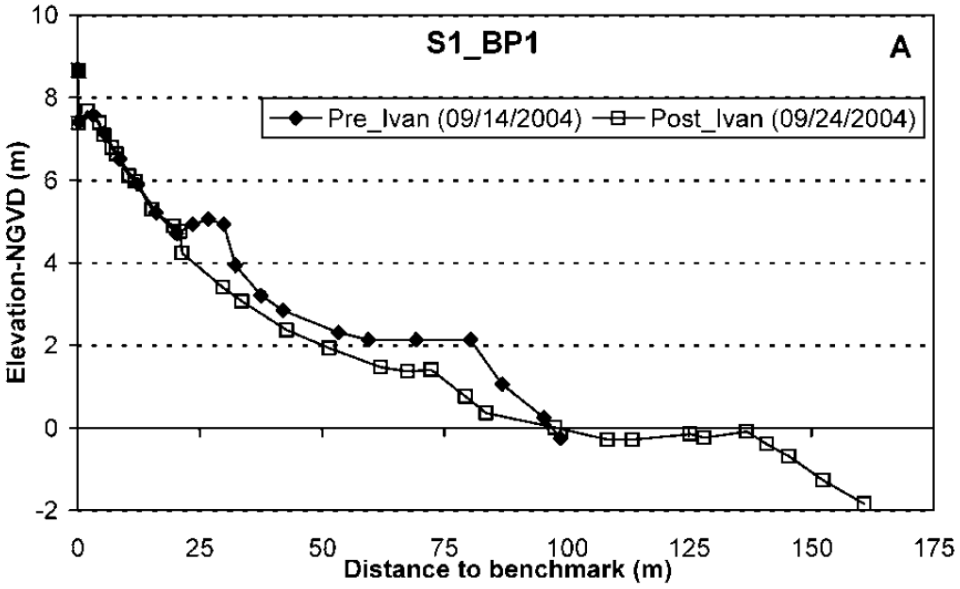

Fig. 2. Pre- and post- storm beach profiles at Beasley Park, USA. (Wang et al., 2006).

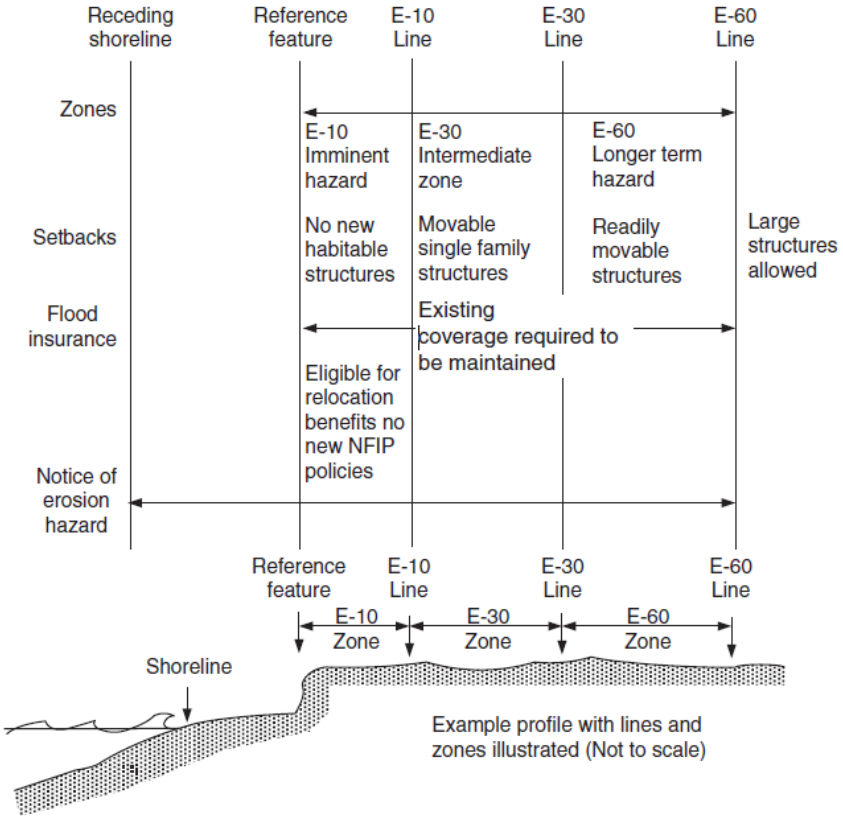

Fig. 3. Scopes of projected erosion lines for various coastal hazard recommended by the NRC in the United States (Dean and Dalrymple, 2002).

2 Numerical Model

XBeach is a 2-D hydrodynamic and morphodynamic model that solves equations for flow, surface waves, sediment transport and bed evolution. Flows are computed by solving the nonlinear shallow water equations. XBeach resolves the individual long waves, while short waves are computed on a group scale with the wave energy spectrum prescribed according to the peak frequency.

The wave forcing in the shallow water momentum equation is obtained from a time dependent version of the wave action balance equation. Similar to Delft University's (stationary) HISWA model (Holthuijsen et al., 1989), the directional distribution of the action density is taken into account whereas the frequency spectrum is represented by a frequency, best represented by the spectral parameter. The wave action balance is then given by:

$$\frac{\partial A}{\partial t}+\frac{\partial C_x A}{\partial x}+\frac{\partial C_y A}{\partial y}+\frac{\partial C_\theta A}{\partial \theta}=-\frac{D_w}{\sigma} \tag{1}$$

with the wave action density:

$$A(x,y,t,\theta)=\frac{S_w(x,y,t,\theta)}{\sigma(x,y,t)} \tag{2}$$

where θ represents the angle of incidence with respect to the x-axis, S_w represents the wave energy density in each directional bin and σ the intrinsic wave frequency. The wave action propagation speeds in x- and y-direction are given by:

$$\begin{aligned} C_x(x,y,t,\theta) &= C_g\cos(\theta)+u^L \\ C_y(x,y,t,\theta) &= C_g\sin(\theta)+v^L \end{aligned} \tag{3}$$

The group velocity C_g is obtained from the linear theory. They are cast into a depth averaged Generalized Lagrangian Mean (GLM) formulation to account for the wave induced mass-flux and the subsequent (return) flow (Andrews and Mcintyre, 1978, Walstra *et al,* 2000). In such a framework, the

momentum and continuity equations are formulated in terms of the Lagrangian velocity, u^L and v^L. This velocity is related to the Eulerian velocity, given by:

$$u^L = u^E + u^S \tag{4}$$

$$v^L = v^E + v^S \tag{5}$$

Here u^S and v^S represent the Stokes drift in x- and y-direction respectively (Phillips, 1977):

$$u^S = \frac{E_w \cos\theta}{\rho h c} \tag{6}$$

$$v^S = \frac{E_w \sin\theta}{\rho h c} \tag{7}$$

The resulting GLM-momentum equations are given by:

$$\frac{\partial u^L}{\partial t} + u^L \frac{\partial u^L}{\partial x} + v^L \frac{\partial u^L}{\partial y} - f v^L - \nu_h \left(\frac{\partial^2 u^L}{\partial x^2} + \frac{\partial^2 u^L}{\partial y^2} \right) = \frac{\tau_{sx}}{\rho h} - \frac{\tau_{bx}^E}{\rho h} - g \frac{\partial \eta}{\partial x} + \frac{F_x}{\rho h} \tag{8}$$

$$\frac{\partial v^L}{\partial t} + u^L \frac{\partial v^L}{\partial x} + v^L \frac{\partial v^L}{\partial y} + f u^L - \nu_h \left(\frac{\partial^2 v^L}{\partial x^2} + \frac{\partial^2 v^L}{\partial y^2} \right) = \frac{\tau_{sy}}{\rho h} - \frac{\tau_{by}^E}{\rho h} - g \frac{\partial \eta}{\partial y} + \frac{F_y}{\rho h} \tag{9}$$

$$\frac{\partial \eta}{\partial t} + \frac{\partial h u^L}{\partial x} + \frac{\partial h v^L}{\partial y} = 0 \tag{10}$$

where τ_{bx} and τ_{by} are the bed shear stresses, η is the water level, F_x and F_y are the wave-induced stresses, υ_t is the horizontal viscosity and f is the Coriolis coefficient. The bottom shear stress terms are calculated with the Eulerian velocities as experienced by the bed:

$$u^E = u^L - u^S \tag{11}$$

$$v^E = v^L - v^S \tag{12}$$

The sediment transport is modeled with a depth-averaged advection diffusion equation [Galappatti and Vreugdenhil, 1985]:

$$\frac{\partial hC}{\partial t} + \frac{\partial hCu^E}{\partial x} + \frac{\partial hCv^E}{\partial y} + \frac{\partial}{\partial x}\left[D_h h \frac{\partial C}{\partial x} \right] + \frac{\partial}{\partial y}\left[D_h h \frac{\partial C}{\partial y} \right] = \frac{hC_{eq} - hC}{T_s} \tag{13}$$

where C represents the depth-averaged sediment concentration which varies on the wave group time scale, and D_h is the sediment diffusion coefficient. The entrainment of the sediment is represented by an adaptation time T_s, given by a simple approximation based on the local water depth, h, and sediment fall velocity w_s:

$$T_s = \max\left(0.05 \frac{h}{w_s}, 0.2 \right) s \tag{14}$$

where a small value of T_s corresponds to nearly instantaneous sediment response. The entrainment or deposition of sediment is determined by the mismatch between the actual sediment concentration, C, and the equilibrium concentration, C_{eq}, thus representing the source term in the sediment transport equation.

The bed-updating is discussed next. Based on the gradients in the sediment transport the bed level changes according to:

$$\frac{\partial z_b}{\partial t} + \frac{f_{mor}}{(1-p)} \left(\frac{\partial q_x}{\partial x} + \frac{\partial q_y}{\partial y} \right) = 0 \tag{15}$$

where p is the porosity, f_{mor} is a morphological acceleration factor of O(1-10) (e.g. Renier et al., 2004a) and q_x and q_y represent the sediment transport rates in x- and y-direction respectively, given by:

$$q_x(x,y,t) = \left[\frac{\partial hCu^E}{\partial x} \right] + \left[\frac{\partial}{\partial x}\left[D_h h \frac{\partial C}{\partial x} \right] \right] \tag{17}$$

$$q_y(x,y,t)=\left[\frac{\partial hCv^E}{\partial y}\right]+\left[\frac{\partial}{\partial y}\left[D_h h\frac{\partial C}{\partial y}\right]\right] \tag{18}$$

To account for bed-slope effects on sediment transport a bed-slope correction factor f_{slope} is introduced.

$$C_{eq}=\frac{A_{sb}+A_{ss}}{h}\left[\left(\left|u^E\right|^2+0.018\frac{u^2_{rms}}{C_d}\right)^{0.5}-u_{cr}\right]^{2.4}(1-\alpha_b m) \tag{18}$$

3 Verifications

To evaluate the reliability of XBeach model, the experimental data by Kajima et al., (1983) were used to validate the numerical simulation on the time evolution of wave deformation and the beach profile change. Their experiments were conducted at the Central Research Institute of Electric Power Industry (CRIEPI) in Japan. The experimental results have been widely used for the verification of the numerical simulations. The referenced experimental water depth (h), the wave height (H), the wave period (T), the slope of the initial seabed (S), and the grain size (D_{50}) employed in the 2-D numerical wave channel are shown in Tab. 1. The schematic diagram of the initial bathymetry for verification is shown as Fig. 4, in which numerical results for the comparison with experimental data are analyzed in the middle section in the y-direction. Fig. 5 shows the comparisons of wave deformation and beach profile with the experimental data by Kajima et al., (1983), in which the left and right column are the case 1-3 and case 3-3 in CRIEPI respectively. The wave deformation including the wave height, the mean water level were presented. It can be seen that the wave height increases due to shoaling and wave set-down occurs before wave breaking. After that, wave set-up causes by wave breaking found from the mean water level (η_{mean}). It's consistent between the experimental data and numerical results in the tendency of coastal erosion and the accretion. The numerical results using XBeach model are in good agreement with the experimental results. These verifications demonstrated that the XBeach model is capable of simulating accurately the wave deformation and the coastal topography change.

Tab. 1. Wave condition for verifications

	CASE1-3	CASE3-3
water depth (h)	4.5m	4.5m
wave height (H)	1.05m	0.81m
wave period (T)	9.0s	12s
slope of the initial seabed (S)	1:20	1:20
grain size (D_{50})	0.47mm	0.27mm

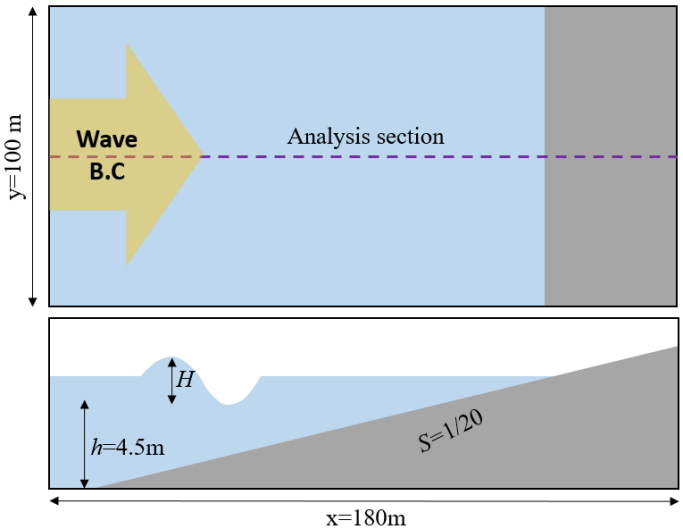

Fig. 4. The schematic diagram of the initial bathymetry for the verification.

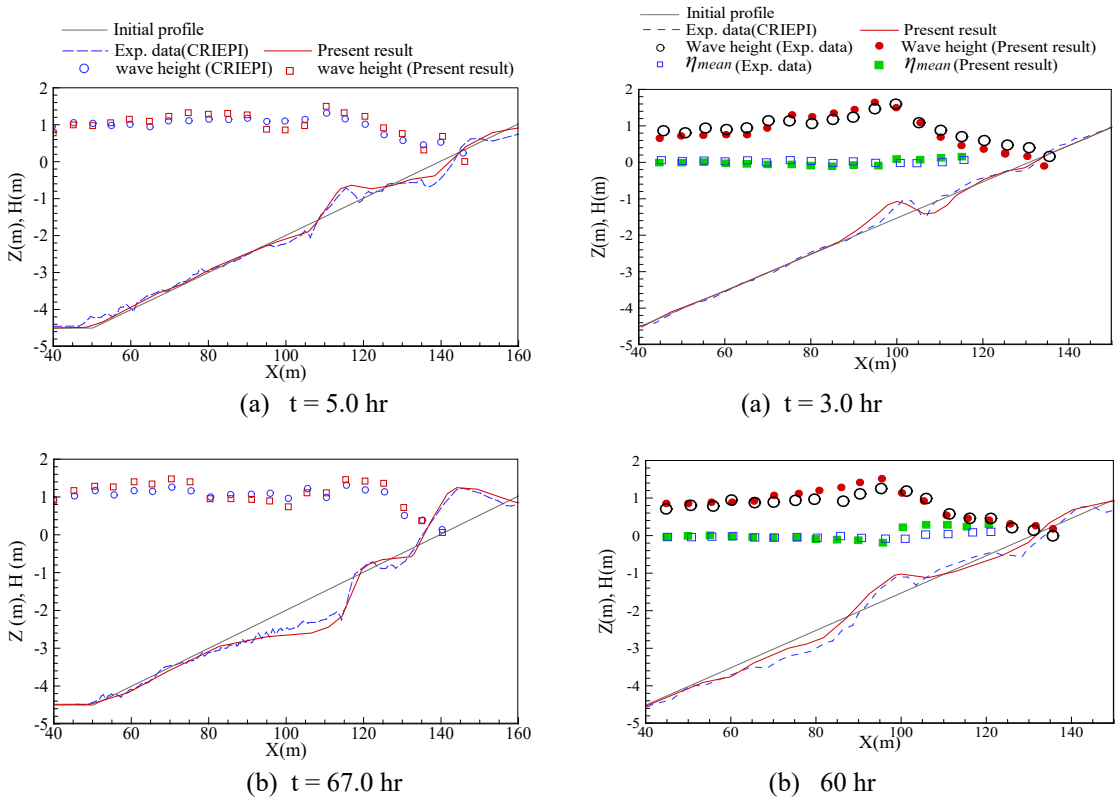

Fig. 5. Comparisons of wave deformation and beach profile. [left: Case1-3 in CRIEPI, right: Case3-3 in CRIEPI]

4 Results and discussion

In this study, we focus on the coastal topography change on an embayed beach and estimate the erosion width under storms with different arrangements of breakwaters. The following simulations by XBeach model include long-term and short-term simulations. The long-term simulation is purposed to obtain the equilibrium shoreline on an embayed beach between breakwaters, which is then applied to be the initial topography condition for the short-term simulation to evaluate the storm-induced erosion.

4.1 Long-term simulation for equilibrium topography

The initial topography is shown in Fig. 6, in which two headlands extends breakwater further into the sea built on a sloping seabed. This two-dimensional sloping seabed is referred from the bathymetry and topographic surveys on the southwestern coast in Taiwan. In which h is the water depth, which is used between -25m and -5m depth with a relative plane 1/50 slope and S=1/40 from -5m depth extended upward to berm (z=+2.5m). The wave condition is H = 1.38 m, T = 5.52 s, and h =25 m compiled from seasonal wave in the SW Taiwan during 1999 and 2013. The initial wave direction is considered 90◦to the shoreline because the wave may be almost parallel to the shoreline caused by wave transformation. Definition of related parameters is shown in Fig. 6. The distance (Xi) between the pier head and the original shoreline is 80m, i.e., the pier head of breakwaters built on the -2m depth, in which the breakwater gap defines Gb. The equilibrium bay shoreline after long-term simulation is shown as red dashed line, and the distance between the pier head and the tangent of downcoast limit is Xe. Referred to arrangements of coastal constructions around the world, e.g., Spain, UK, Denmark, and the USA, the value of the simple ratio (Xi/Gb) is between 0.5~1.5 (Khuong, 2016). Therefore, the values of Xi/Gb=0.5~1.5 are firstly used to calculate the long-term simulation in this study. In this study, the numerical results for the case (Xi/Gb=1) are following to explain the detail, and a comprehensive comparison for all cases (Xi/Gb=0.5~1.5) will be displayed at last.

The simulated time evolutions of the Xe and the profile change at section A on an embayed beach (Xi/Gb=1) are shown in Fig. 7. It can be seen that the setback width of initial shoreline approaches to

the equilibrium status after seasonal wave acting 50 days. The Fig. 7(b) indicates the cross-section profile changes show in a good agreement with the EBP (Equilibrium Beach Profile) which was established by Dean(1977, 1991). Fig. 8 displays the two-dimensional distribution of wave height, nearshore current field, and the equilibrium bay bathymetry. Fig. 8(a) displays that the leeside of the breakwaters becomes a sheltering region due to wave diffraction by the headland effect. Diffraction is regarded as a key process capable of modifying the wave direction around the headland, and the wave decays results in the gradient of wave height. The current system was induced by the radiation stress, in which the symmetric circulation pattern of current can be found in the shadow zone in lateral sides and the rip system is distinctively cross-shore oriented on the central coastal zone shown in Fig. 8(b). The wave-induced current can drive the sediment transport to cause the curvature of the shoreline on an embayed beach illustrated. The coastal topography change is shown in Fig. 8(c), in which the dark gray contour solid line displays the bathymetry at 1-m interval between –5m and +1 elevation. It can be seen that the erosion happens in the gap region, and the accretion occurs along the breakwaters in the lateral sides. The red solid line and blue dashed line indicate the numerical equilibrium bay shoreline and the parabolic bay shape equation (PBSE) derived by Hsu and Evans (1989), respectively. The comparison with PBSE evidences the numerical equilibrium shoreline is approximated to the parabolic empirical formula.

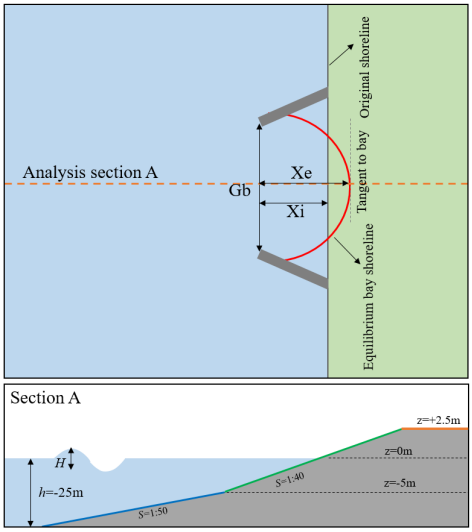

Fig. 6. A schematic diagram of the physical 2-D model for the long-term simulation in the present study

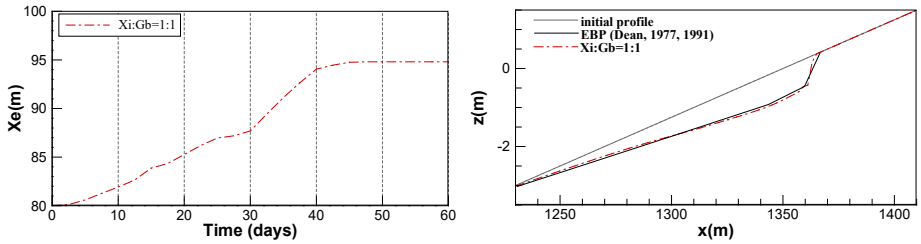

[a] time evolutions of the Xe [b] cross-section profile change

Fig. 7. The time evolutions of the Xe (a) and the section-profile change (b) on a sloping seabed under seasonal wave condition (at section A).

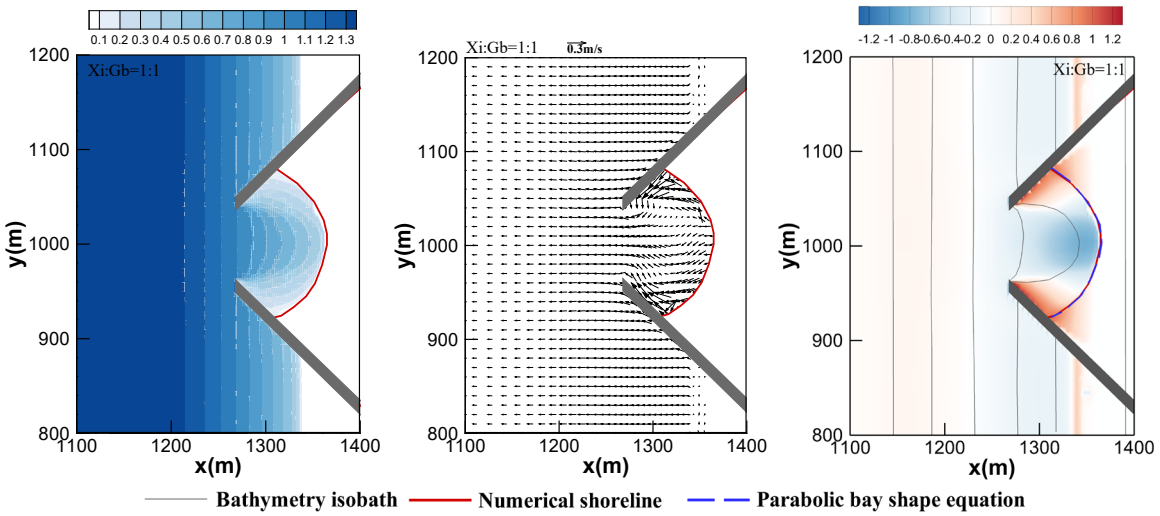

[a] wave height [b] current velocity [c] topography change

Fig. 8. The two-dimensional distribution of wave height, flow field and topography bathymetry of equilibrium beach profile.

4.2 Short-term simulation for estimating storm beach buffer width

This study applies the topography of the equilibrium shoreline on an embayed beach as the initial condition to evaluate the storm-induced erosion width for short-term storm wave action. Offshore wave conditions derived from storms of 10-, 20- and 50- year return periods for south-western Taiwan are considered in this study. Referring to Lee et al. (2011), the offshore wave conditions and design water levels of different return periods are shown in Tab. 2. As the storm waves impact in an embayed beach with normal incidence, it may cause fierce erosion on the gap between the breakwaters. To assess the erosion width during storms for the safe application of the coastal protection in the future, the extreme situation is taken into account. Thus, the normal wave incidence of storms is considered in this study.

Fig. 9 displays the distribution of wave height, nearshore current field, and beach topography change after 48 hours of action by the RP-10 and RP-50 storms. The headland effect can be seen when the storm waves propagate behind the breakwater, and the waves decay at the leeside to be sheltering region. The distribution of wave field is all along the bay almost parallel to the bathymetry isobaths. Two main circulation cells can be found behind the breakwaters, and the current systems flow along with the structure in lateral sides shown in Fig. 9(b). It is noted that the current system will be derived into the outgoing rip current and inflow current near the pier head different from the seasonal wave condition in Fig. 8(b). When comparing the current system between RP-10 and RP-50, it can be found that the stronger nearshore current circulation happens over the stronger wave action. The topography change is shown in Fig. 9(c), in which the gray solid contour lines and blue dashed contour lines illustrate the isobaths bathymetry at 1-m interval between –2m and +2 elevation in equilibrium and after storm acting, respectively. The erosion level displays the maximum erosion elevation of the storm action, i.e., the coastal change is zero, illustrated in dark blue dashed contour line. The topography change is significant behind the breakwaters particularly. Erosion phenomenon happens in the region at the gap, and the accretion will be found at the leeside along the breakwaters, respectively.

Tab. 2. Offshore wave conditions of different return periods for short-term storm simulation.

Wave condition / Return period	*H*(m)	*T*(S)	Design water level (m)
10 years	5.22	9.45	1.17
20 years	5.67	9.86	1.27
50 years	7.02	10.97	1.39

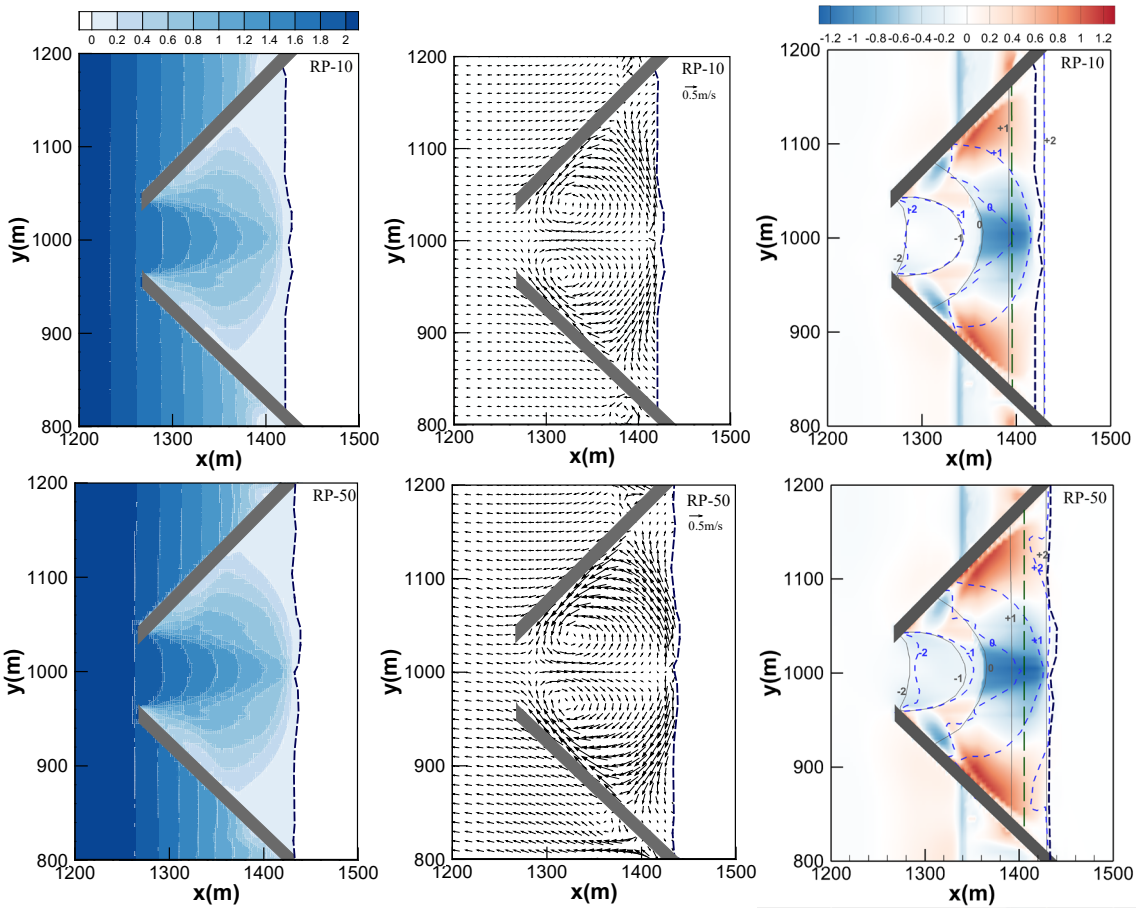

Fig. 9. The comparisons of wave height, flow field and topography bathymetry of equilibrium beach by different storm return period for short-term simulation.

The definition of the storm beach buffer width (Xb), the erosion width of the shoreline (Xs) are illustrated in Fig. 10. The Xd is the distance between the design water level corresponding to storm return period and the erosion level. The relationship between storm buffer width Xb, the erosion width Xs, and the Xd over different storm return periods acting on an embayed beach (Xi/Gb=1) are obtained and shown in Fig. 11. The results depict that the larger storm beach buffer width for larger cyclonic waves is needed for the coastal protection. Moreover, to analyze the relationship with erosion phenomenon and the geometric arrangement of breakwaters, a comprehensive comparison with Xb, Xs, Xd, and Xi/Gb=0.5~1.5 over the storm of 50- year return period is investigated. The normalized parameters, e.g., Xb/Gb, Xs/Gb, Xd/Gb and Xi/Gb are shown in Fig. 12. As the Xi/Gb increases (i.e. the distance of the gap decreases), the shoreline after the storm will setback obviously and the larger storm beach buffer width will be needed. Mainly due to the narrower gap, the fiercer current system and the erosion phenomenon may occur within an embayed beach as the storm impact with the same intensity. These erosion characteristics with different storm return periods and geometric arrangements can evaluate the appropriate width for coastal protection design.

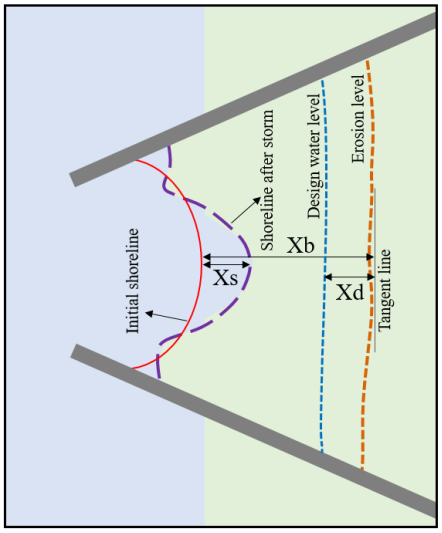

Fig. 10. Definition of storm beach width Xb, Xd and Xs for an embayed beach.

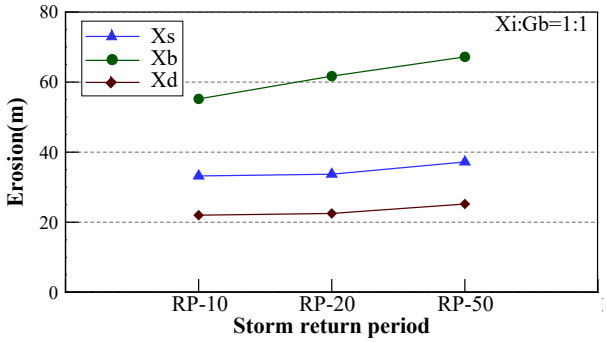

Fig. 11. The relationship between storm buffer width Xb, the erosion width Xs, Xd and different return periods.

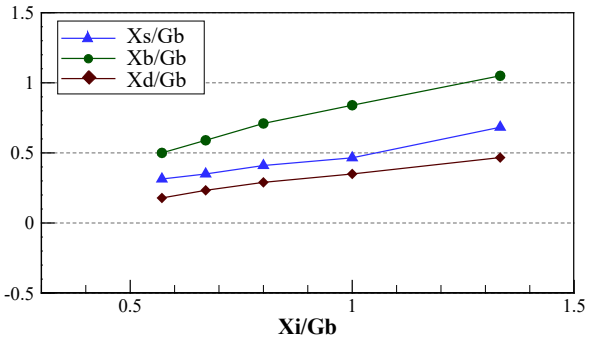

Fig. 12. The normalized parameters between Xb/Gb, Xs/Gb, Xd/Gb and Xi/Gb.

5 Conclusions

This study applies a two-dimensional XBeach model to simulate the coastal topography change under storm wave action and simulations of storm-induced erosion on an embayed beach. The previous experimental data (Kajima et al., 1983) were applied to validate the numerical model, and the numerical results show in a good agreement with the experiments. The XBeach model was then employed to perform the topography with equilibrium shoreline on an embayed beach based on long-term simulation. The equilibrium bay shoreline curve is approximated to the parabolic bay shape equation (PBSE) derived by Hsu and Evans (1989). The storm beach change on an embayed beach was then simulated using the topography of equilibrium shoreline as the initial condition under storm wave action.

The results over storm wave show two main circulation cells can be found behind the breakwaters, and the stronger nearshore current circulation happens over the stronger wave action. Erosion phenomenon happens in the region at the gap, and the accretion will be found at the leeside along the breakwaters, respectively. We defined the distance of beach erosion measured from the original equilibrium shoreline as the storm beach buffer width for shore protection behind the offshore breakwater. The storm buffer width on an embayed beach (Xi:Gb=1:1) was obtained for three storm waves with 10-, 20-, and 50-year return periods. The results depict that the larger storm beach buffer width for larger cyclonic waves is needed for the coastal protection. Moreover, as the distance of the gap decreases (Xi/Gb=0.5~1.5), the shoreline after the storm will setback obviously and the larger storm beach buffer width will be needed due to the fiercer current system mainly.

References

Andrews, D.G., McIntyre, M.E., 1978a. An exact theory of nonlinear waves on a Lagrangian-mean flow. Journal of Fluid Mechanics, 89 (4), 609–646.

Andrews, D.G., McIntyre, M.E., 1978b. On wave-action and its relatives. Journal of Fluid Mechanics, 89 (4), 647–664.

Daly, C.J., Bryan,K.R., Winter,C., 2014. Wave energy distribution and morphological development in and around the shadow zone of an embayedbeach. Coastal Engineering, 93, 40–54.

Dean, R.G., 1977. Equilibrium beach profiles: U. S. Atlantic, Gulf coasts. Ocean Engineering Report No.12, Department of Civil Engineering, University of Delaware, Newark, Delaware, 45.

Dean, R.G., (1991). Equilibrium beach profiles: characteristics and applications. Journal of Coastal Research, 7, 53-84.

Dean, R.G., R. A. Dalrymple, 2002. Coastal processes with engineering application. Cambridge University Press; United Kingdom.

Galappatti, R., Vreugdenhil, C.B., 1985. A depth integrated model for suspended transport. Journal of Hydraulic Research, 23 (4), 359-377.

Holthuijsen, L.H., Booij N., Herbers T.H.C., 1989. A prediction model for stationary, short-crested waves in shallow water with ambient currents. Coastal Engineering, 13, 23-54.

Hsu, J.R-C., Evans, C., 1989. Parabolic Bay Shapes and Applications, in:Proceedings of the Institution of Civil Engineers, Part 2, Vol. 87. pp. 557-570.

Kajima, R., Shimizu, T., Maruyama, K., Saito, S., 1983. On-offshore sediment transport experiment by using large scale wave flume. Collected data No. 1-8, Central Research Institute of Electric Power Industry, Japan (in Japanese).

Khuong, T.C., 2016. Shoreline response to detached breakwaters in prototype. Dissertation Delft, Faculty of Civil Engineering and Geosciences, Department of Hydraulic Engineering.

Lee F. C., J. R. C. Hsu, W. H. Lin, 2011. Appraisal of storm beach buffer width for cyclonic waves. Coastal Engineering, 58, 1049-1061.

Loureiro, C., Ferreira, Ó., Cooper, J.A.G., 2012a. Extreme erosion on high-energy embayed beaches : influence of megarips and storm grouping. Geomorphology. 139–140, 155–171.

Loureiro, C., Ferreira, Ó., Cooper, J.A.G., 2012b. Geologically constrained morphological variability and boundary effects on embayed beaches. Marine Geology. 329–331, 1–15.

Phillips, O.M., 1977. The dynamics of the upper ocean (2nd ed.). Cambridge University Press; United Kingdom.

Reiner A, Perkel D.J., Bruce L.L., Butler A.B., Csillag A., Kuenzel W., Medina L., Paxinos G., Shimizu T., Striedter G., Wild M., Ball G.F., Durand S., Gunturkun O., Lee D.W., Mello C.V., Powers A., White S.A., Hough G., Kubikova L., Smulders T.V., Wada K., Dugas-Ford J., Husband S., Yamamoto K., Yu J, Siang C., Jarvis E.D., 2004a. Revised nomenclature for avian telencephalon and some related brainstem nuclei. Journal of Comparative Neurology.473, 377–414.

Silvester, R. and J.R.C. Hsu, 1993. Coastal Stabilization:Innovative Concepts. Englewood Cliffs, NJ: Prentice Hall, 578.

Walstra, D.J.R., Roelvink, J.A., Groeneweg, J., 2000. Calculation of wave-driven currents in a 3D mean flow, in: Proceedings of 27th International Conference on Coastal Engineering, Sydney. ASCE, Reston, VA, pp. 1050-1063.

Wang, P., Kirby, J.H., Haber, J.D., Horwitz, M.H., Knorr, P.O., Krock, J.R., 2006. Morphological and sedimentological impacts of Hurricane Ivan and immediate poststorm beach recovery along the northwestern Florida barrier-island coasts. Journal of Coastal Research 22 (6), 1382–1402.

Yasso, W.E., 1965. Plan Geometry of Headland-Bay Beaches. The Journal of Geology, 73, 702-714.